Statistical Rate Theory Determination of Water Properties below the Triple Point

ARTICLE *in* THE JOURNAL OF PHYSICAL CHEMISTRY B · AUGUST 2008

Impact Factor: 3.3 · DOI: 10.1021/jp711768w · Source: PubMed

3 AUTHORS, INCLUDING:

Fei Duan
Nanyang Technological University
24 PUBLICATIONS **315** CITATIONS
SEE PROFILE

Charles Albert Ward
University of Toronto
141 PUBLICATIONS **2,585** CITATIONS
SEE PROFILE

Statistical Rate Theory Determination of Water Properties below the Triple Point

Fei Duan, Ian Thompson, and C. A. Ward*

Department of Mechanical and Industrial Engineering, University of Toronto, Toronto, Canada M5S 3G8

Received: December 14, 2007; Revised Manuscript Received: April 22, 2008

We report a new method for determining the saturation vapor pressure, $P_s(T)$, of water at conditions below its triple point. $P_s(T)$ appears as a parameter in the statistical rate theory (SRT) expression for the net evaporation flux. We use measurements of the interfacial conditions during steady-state evaporation and condensation experiments and SRT to determine the values of $P_s(T)$ from 50 different experiments over a range of interfacial conditions. From these values of $P_s(T)$, we develop an analytical expression and from it calculate the liquid−vapor latent heat, $L_{lv}(T)$, and the constant pressure specific heat, $c_p^L(T)$. The calculated values of these properties are compared with those obtained from independent measurements. This comparison indicates the SRT expressions for $L_{lv}(T)$ and $c_p^L(T)$ are consistent with the measurements over a range of temperatures.

1. Introduction

One of the troubling questions in previous measurements of the saturation vapor pressure, $P_s(T)$, for water, at temperatures below its triple point, is whether the absence of equilibrium has affected the values recorded. The saturation vapor pressure is strictly defined as the pressure at which the isothermal liquid and its vapor are in equilibrium while in contact across an interface that is free of curvature. But none of the measurements of $P_s(T)$, made at temperatures below the triple point, have held the liquid and vapor phases in this condition and measured $P_s(T)$. Since the liquid phase is metastable in this temperature range,[1] the measurements are bedeviled by the possibility of ice formation.

The technique adopted by Bottomley[2] to measure $P_s(T)$ was to have a sample of water in each of two connected glass bulbs, to induce freezing in one bulb and maintain both bulbs at the same temperature. He considered the saturation vapor pressure of ice to be known and measured the pressure difference between the two bulbs. Strictly speaking, the system used by Bottomley could not have been in equilibrium. Since the water sample had a higher pressure than the vapor, there would have been molecular transport from the water sample bulb to the bulb containing ice. This means the water sample was evaporating and condensation was occurring on the ice. The values of $P_s(T)$ reported by Bottomley are shown in Figure 1.

Kraus and Greer[3] measured the pressure in the vapor phase contacting (what they assumed were) small water droplets (dew), but it was not possible for them to directly observe the droplets, so some of the droplets could have been ice (frost). In Figure 1, the results of Kraus and Greer are also shown. At the lowest temperature considered by Bottomley, 258.7 K, the value of $P_s(T)$ reported by Kraus and Greer is 14% greater than that of Bottomley, and generally that relation exists between the two sets of data. However, Kraus and Greer felt that their measurements were anomalously low in the temperature range from 251.4 to 254.5 K. If a portion of the droplets in their experiments were frozen, one could reasonably expect the vapor-phase pressure to have been less than would have been the case if only liquid droplets were present.

* Corresponding author. E-mail: ward@mie.utoronto.ca.

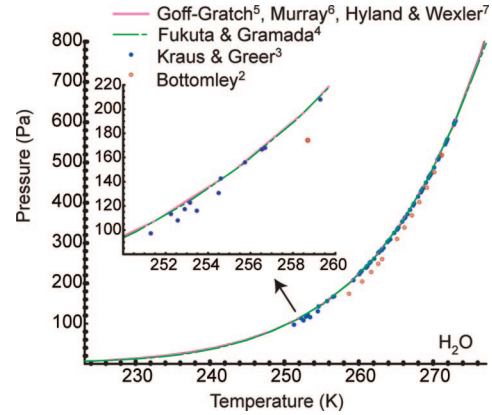

Figure 1. Comparison of reported values of the saturation vapor pressure.

Fukuta and Gramada[4] made measurements of $P_s(T)$ below the triple point and proposed an analytical expression for $P_s(T)$. They had ice in one portion of their system and cooled a surface near the ice until water droplets formed on the cooled surface. They recorded the temperature of the ice and the temperature of the cooled surface. To analyze their data, they assumed equilibrium and set the molecular flux from the ice and from the water equal. Strangely, they also assumed the square of the molecular speed—not the average of the square of the molecular speed, as normally used in kinetic theory—is proportional to the temperature. Their data show a scatter of at least 5% near 253 K, but the analytical expression they propose for $P_s(T)$ is not a fit of their data. They chose their larger measured values of $P_s(T)$ to form their analytical expression.

In Figure 1, we show the values of $P_s(T)$ calculated from four proposed analytical expressions, including that of Fukuta and Gramada.[4–7] The analytical expressions are in close agreement with one another, but not with the data.[8] For temperatures below 254.5 K, the measurements of Kraus and Greer are clearly below the analytical expressions, and the data of Bottomley are below the analytical expressions for all the temperatures he considered. However, one cannot be sure of the validity of the analytical expression for $P_s(T)$, since for temperatures below the triple point, the calculations are based on extrapolations. For example, the Goff−Gratch[5] equation was obtained by

10.1021/jp711768w CCC: $40.75
Published on Web 06/26/2008

integrating the Clausius−Clapeyron equation and evaluating the coefficients from data available in the temperature range between 273.15 and 373.15 K. Thus, when these calculations are applied below the triple point, an extrapolation is being made that is outside of the data range.[8]

Generally, the analytical expressions show a different slope than the data. Since the latent heat, $L_{lv}(T)$, can be calculated using the Clausius−Clapeyron equation when $P_s(T)$ is given, and the calculated values depend on the slope of the $P_s(T)$ curve, this difference in slope is magnified when a comparison of $L_{lv}(T)$ values is made with independent measurements of $L_{lv}(T)$.[9,10] The disagreement is more severe for some $P_s(T)$ expressions than for others. Further, the constant pressure specific heat of the liquid phase, $c_p^L(T)$, can be determined by further differentiation of the $P_s(T)$ expression. All but one of the previous analytical expression for $P_s(T)$ are shown to lead to values of either $L_{lv}(T)$ or $c_p^L(T)$ that are in disagreement with the data.

We propose to determine the expression for $P_s(T)$ for water at temperatures below its triple point from measurements made during evaporation and condensation experiments and a theory of kinetics, statistical rate theory (SRT),[11–33] that contains the equilibrium property $P_s(T)$ as a parameter but no undefined or fitting parameters.[18]

A new series of water evaporation experiments are reported in which water was maintained at the mouth of a poly methyl methacrylate (PMMA) funnel while it evaporated into its own vapor. In these experiments water was visible from outside the evaporation chamber, and its state could be determined at any time by dipping a thermocouple into the water. In the PMMA funnel, water could be maintained liquid down to 253.89 K while the vapor was at 127.3 Pa. When ice nucleation occurred, there was a sharp rise in both temperature and pressure. When these experimental results are added to other evaporation and condensation experiments that have been reported in the literature[18–21] and SRT is used to determine the value of $P_s(T)$ from each experiment, an analytical expression for $P_s(T)$ can be formulated that is in close agreement with the values of $P_s(T)$ determined from SRT. When the values of $L_{lv}(T)$ and $c_p^L(T)$ calculated from the SRT expression for $P_s(T)$ are compared with independent measurements of $L_{lv}(T)$ and $c_p^L(T)$ there is better agreement than with the other analytical expressions down to 253.89 K. Below this temperature the data for $c_p^L(T)$ are not consistent.

2. Determination of $P_s(T)$ from Measurements Made under Nonequilibrium Conditions

Previous studies of the conditions at the interface during evaporation or condensation have indicated that independently of the direction of the net molecular transport, the interfacial temperature in the vapor is greater than that in the liquid.[18–22,24,25,34–36] The physical idea that emerges from these studies is that during evaporation it is the higher energy molecules that escape the liquid and during condensation it is the lower energy molecules that are captured by the liquid.[19] In both cases then, the higher energy molecules are in the vapor phase at the interface; thus, the higher temperature there. In the SRT approach, the transition probability concept of quantum mechanics is used to predict the probability of these events, and as might be expected, the result comes out in terms of the change in entropy that results from a molecule transferring from the liquid to the vapor phase, Δs_{LV}. When the assumption that the molecular exchange rate between the possible quantum states is the same is added, an expression for the net evaporation rate, j_{ev}, is obtained that is free of undefined parameters (fitting constants). If the equilibrium exchange rate between the phases is denoted K_e, the net rate of molecular flux from the liquid to the vapor phase is given by[18,23]

$$j_{ev} = 2K_e \sinh\left(\frac{\Delta s_{LV}}{k_B}\right) \tag{1}$$

where k_B is the Boltzmann constant. If the chemical potentials of the molecules in the liquid and the vapor phases at the interface are denoted μ_I^L, μ_I^V, the interfacial temperatures as T_I^L, T_I^V, and the interfacial enthalpy of the vapor as h_I^V, then[23]

$$\Delta s_{LV} = \left(\frac{\mu_I^L}{T_I^L} - \frac{\mu_I^V}{T_I^V}\right) + h_I^V\left(\frac{1}{T_I^V} - \frac{1}{T_I^L}\right) \tag{2}$$

Note that the SRT expression for j_{ev} allows both the chemical potential and the temperature to be discontinuous across the interface.

The saturation vapor pressure enters the theory as the reference condition at which the chemical potentials of the molecules in the liquid and vapor phases are equal when the pressures and temperatures in each phase have the same value:

$$\mu^L[T, P_s(T)] = \mu^V[T, P_s(T)] \tag{3}$$

If the isothermal compressibility κ_T is such that $|\kappa_T(P^L - P_s)| \ll 1$, the chemical potential of the liquid phase may be expressed

$$\mu^L(T^L, P^L) = \mu^V[T^L, P_s(T^L)] + v_f(T^L)[P^L - P_s(T^L)] \tag{4}$$

where $v_f(T^L)$ is the specific volume at the saturation condition. For the conditions we consider, we suppose the vapor-phase pressure to be less than $P_s(T_I^V)$. This allows the vapor phase to be approximated as an ideal gas (see below).

$$\mu^V(T^V, P^V) = \mu^V[T^L, P_s(T^L)] + k_B T^V \ln\left[\frac{P^V}{P_s(T^V)}\right] \tag{5}$$

Under equilibrium conditions, we take the equilibrium exchange flux, K_e, to be equal to the flux of vapor-phase molecules to the interface. If T_e and P_e^V denote the equilibrium temperature and the equilibrium pressure in the vapor phase, and the mass of the water molecule is denoted m_w, then

$$K_e = \frac{P_e^V}{\sqrt{2\pi m_w k_B T_e}} \tag{6}$$

and since $\mu^L(T_e, P_e^L)$ and $\mu^V(T_e, P_e^V)$ are equal when equilibrium is reached, one finds from eqs 4 and 5

$$P_e^V = P_s(T_e)\exp\left[\frac{v_f}{v_g}\left(\frac{P^L}{P_s(T_e)} - 1\right)\right] \tag{7}$$

where v_g is the specific volume of the vapor at equilibrium.

If a phase-change process is taking place at the liquid−vapor interface with $T_I^L \neq T_I^V$ and the portions of the system at the interface that are approximated as being in local equilibrium are isolated and allowed to come to true equilibrium, we take as an approximation[18]

$$T_e = T_I^L \tag{8}$$

Then from eqs 6–8 the expression for the equilibrium molecular exchange flux is

$$K_e = \frac{P_s(T_I^L)\exp[(v_f/v_g)(P^L/P_s(T_I^L)-1)]}{\sqrt{2\pi m_w k_B T_I^L}} \quad (9)$$

If the local equilibrium approximation is valid in the liquid and vapor phases at the interface, statistical thermodynamics may be applied to determine the expressions for μ_I^V and h_I^V. If the fundamental vibration frequencies of the triatomic water molecule are denoted as ω_l, the expression for Δs_{LV} may be written[18,19,23]

$$\frac{\Delta s_{LV}}{k_B} = 4\left(1-\frac{T_I^V}{T_I^L}\right)+\left(\frac{1}{T_I^V}-\frac{1}{T_I^L}\right)\sum_{l=1}^{3}\left(\frac{\hbar\omega_l}{2k_B}+\frac{\hbar\omega_l}{k_B[\exp(\hbar\omega_l/k_B T_I^V)-1]}\right)+\frac{v_f}{k_B T_I^L}[P_I^V+\gamma^{LV}(C_1+C_2)-P_s(T_I^L)]+\ln\left[\left(\frac{T_I^V}{T_I^L}\right)^4\left(\frac{P_s(T_I^L)}{P_I^V}\right)\right]+\ln\left(\frac{q_{vib}(T_I^V)}{q_{vib}(T_I^L)}\right) \quad (10)$$

where γ^{LV} is the surface tension, C_1 and C_2 are the interface curvatures, and

$$q_{vib}(T) \equiv \prod_{l=1}^{3}\frac{\exp(-\hbar\omega_l/2k_B T)}{1-\exp(-\hbar\omega_l/k_B T)} \quad (11)$$

The vibration frequencies of the covalent bonds of the water molecule involve combinations of symmetric stretch (3651 cm^{-1}), asymmetric stretch (3756 cm^{-1}), and bending (1590 cm^{-1}).[37]

When eqs 10 and 9 are combined with eq 1, one obtains an expression for the evaporation flux that is in terms of the instantaneous interfacial properties T_I^L, T_I^V, P_I^V, P_I^L, the material properties of water $P_s(T_I^L)$, v_f, γ^{LV}, and the internal vibration frequencies of the water molecule, ω_l. We take the material properties v_f and γ^{LV} and the internal vibration frequencies to be known from previous, independent experiments (see below). We measure the values of the instantaneous interfacial properties and j_{ev}. Since there are no free or fitting parameters in the SRT equation for the evaporation flux, the value of $P_s(T_I^L)$ is the only unknown in the system of equations, and its value may then be numerically determined.

3. Experimental Methods

In preparation for an experiment, the water to be used was deionized, distilled, and nanofiltered. Afterward, the resistivity of a sample was 18.2 M Ω·cm and its surface tension was within 1% of the documented value at the temperature of the measurement. A sample of the prepared water was introduced into a glass flask and degassed for at least 24 h while being stirred. No residual gas could be measured after the degassing process. During the degassing period, the vacuum chamber and the syringe of a pump were evacuated with a turbomolecular pump, reaching a pressure of ~10^{-5} Pa (see Figure 2). The degassed water was transferred directly into the syringe of the pump without exposure to air.

The syringe was connected to the throat of a funnel that was enclosed in the vacuum chamber. The funnel had a mouth opening of 7 mm, and the funnel was constructed of PMMA (see Figure 2). Water was pumped from the syringe into the funnel until the maximum height of the water above the funnel mouth was 1.0 mm. At this height, the water−vapor interface was very nearly spherical. To prevent subsequent bubble formation, with water filling the funnel, the chamber was pressurized with N_2 to ~140 kPa for at least 12 h. Afterward, 2.5 mL of liquid was flushed out of the 0.05 mL funnel in order to remove any water containing dissolved N_2. The chamber was dried with a mechanical vacuum pump that was separated from the chamber by a cold trap.

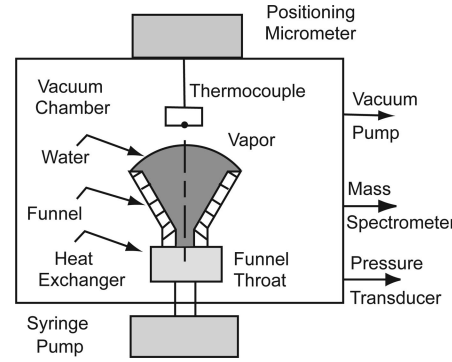

Figure 2. Schematic of the experimental apparatus.

TABLE 1: Thermal Conditions in Liquid and Vapor Phases on the Funnel Centerline Measured during Steady-State Evaporation[a]

experiment	vap phase pressure Pa	evap flux g/m² s	vap intf temp K	liq int temp K	intf radius R_1 mm	intf radius R_2 mm
ET1	127.3	0.494	257.74	253.89	6.740	6.740
ET2	168.3	0.548	259.51	256.23	6.625	6.625
ET3	188.3	0.487	260.60	257.55	6.625	6.625
EV1	797.2	0.027	278.10	276.85	6.740	6.740
EV2	795.7	0.034	278.03	276.91	6.625	6.625
EV3	786.8	0.043	277.77	276.67	6.740	6.740
EV4	791.5	0.050	277.80	276.72	6.682	6.682
EV5	787.9	0.056	277.83	276.71	6.569	6.569
EV6	786.6	0.063	277.77	276.71	6.462	6.462
EV7	783.9	0.066	277.71	276.62	6.799	6.799
EV8	777.3	0.069	277.61	276.50	6.625	6.625
EV9	770.1	0.075	277.50	276.41	6.799	6.799
EV10	765.3	0.076	277.35	276.26	6.625	6.625
EV11	745.3	0.139	277.88	275.88	6.625	6.625
EV12	665.3	0.235	276.52	274.26	6.358	6.358
EV13	591.9	0.346	274.99	272.62	6.569	6.569
EV14	505.3	0.508	272.95	270.33	6.860	6.860
EV15	398.6	0.733	270.50	267.11	6.625	6.625
EV16	301.3	0.931	267.49	263.48	6.569	6.569
EV17	285.3	1.167	265.96	261.54	6.625	6.625
EV18	264.0	1.142	265.84	261.29	6.682	6.682
EV19	258.6	1.205	265.56	261.09	6.625	6.625

[a] Refs 20 and 34.

The water−vapor interface could be viewed from outside the chamber with a cathetometer. With degassed water in the funnel, the pressure in the chamber was reduced with the mechanical vacuum pump and the rate at which water was pumped with a syringe pump into the funnel was adjusted until the system had reached steady state. The evaporation was assumed to be at steady state if the height of the liquid−vapor interface did not vary by more than ±10 μm during the course of the measurements. With the water−vapor interface unmoving, the evaporation rate is equal to the pumping rate. The syringe pump provided a flow rate that had an accuracy of 0.5% of the indicated pumping rate.

As the water passed through the funnel throat, its temperature was brought to 276.7 K by the heat exchanger and its temperature was monitored by a thermocouple placed at the funnel throat. Since water has its maximum density at 277.15 K, further cooling by evaporation at the water−vapor interface made the water there lighter and, thus, eliminated buoyancy-driven convection during the evaporation experiments.

The vapor phase was monitored with a quadrupole mass spectrometer both before and after an experiment. Air was the only impurity identified. The partial pressure of N_2 was $\sim 8 \times 10^{-5}$ Pa, and the partial pressure of H_2O was at least 6 orders of magnitude larger.

Once the water was evaporating steadily, the temperature in the vapor and liquid phases was measured with a calibrated thermocouple (type K, 25 μm diameter wire, 45 μm diameter bead) that had been formed into a U-shape. It was mounted on a positioning micrometer that could be placed at a position with an accuracy of ± 10 μm. The temperature was measured on the funnel centerline in the liquid and vapor phases as a function of height. The interfacial vapor temperature was measured by placing the centerline of the thermocouple bead 30 μm above the interface, and in the liquid phase the interfacial liquid was measured by placing the bead 30 μm below the interface. We neglect any variation of the temperature within the thermocouple bead and take the temperature measured at these positions to be the temperature at that point.

The temperature was measured by placing the calibrated thermocouple at a position using the positioning micrometer and recording the thermocouple output every second for a period of 30 s using a data acquisition system. The mean and standard deviation of the thermocouple readings made at each position were recorded. The error in a temperature reading is taken to be the standard deviation of the temperatures measured at a point.

4. Experimental Results

The type of temperature profile measured on the centerline is shown in Figure 3. Note the temperature discontinuity at the water−vapor interface. Such a temperature discontinuity has been seen in a number of other evaporation and condensation experiments, including liquids other than water.[18–22,25,34–36]

The pressure in the vapor phase 19 cm above the liquid−vapor interface was measured with a Hg manometer and a cathetometer. The measurement had an accuracy of ± 13.3 Pa. The pressure in the liquid phase at the interface was calculated from the Laplace equation. If the curvature of the spherical interface is denoted C_0, then

$$P_I^L = P_I^V + 2\gamma^{LV}(T_I^L)C_0 \tag{12}$$

and since the water−vapor interface was spherical, C_0 may be expressed in terms of the funnel radius, x_m, and the maximum height of the interface above the funnel mouth, z_m:

$$C_0 = \frac{2z_m}{z_m^2 + x_m^2} \tag{13}$$

The value of z_m was measured in each experiment, and x_m was 3.5 mm.

Although surface tension-driven convection can be present during water evaporation,[19–21,34,35] for experiments conducted in which the temperature at the interface is less than that at the funnel throat, the conduction through the solid funnel walls makes the temperature at the periphery of the water−vapor interface, where it contacts the funnel mouth, higher than that on the centerline of the funnel. As a result there can be surface tension-driven convection from the periphery toward the centerline; however, the centerline is a stagnation point for this convection because of its axisymmetric nature. Also, in the case we are considering, since the thermal conductivity of PMMA is less than half that of water, thermal conduction to the periphery of the water−vapor interface is expected to have a negligible effect on the temperature there. Thus, on the centerline, convective effects may be neglected and the local evaporation flux there may be determined from the Stefan condition:

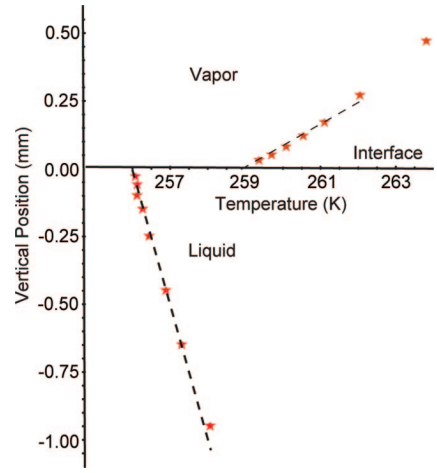

Figure 3. Water was maintained at the mouth of a PMMA funnel, see Figure 2.As water evaporated steadily, the temperature on the funnel centerline was measured as a function of height in the liquid and vapor phase.

$$j_{ev} = \frac{(-\kappa^L \nabla T^L \cdot \iota_r + \kappa^V \nabla T^V \cdot \iota_r)}{h^V(T_I^V) - h^L(T_I^L)} \tag{14}$$

The enthalpies h^V and h^L are evaluated at different temperatures. Their differences may be evaluated by introducing the constant pressure specific heats in the liquid and vapor phases and calculating their change from that at the triple point temperature, T_{tp}. If their difference at the triple point is denoted $h_{fg}(T_{tp})$, then

$$h^V(T_I^V) - h^L(T_I^L) = h_{fg}(T_{tp}) + c_p^V(T_I^V - T_{tp}) - c_p^L(T_I^L - T_{tp}^L) \tag{15}$$

We use the values of $h_{fg}(T_{tp})$, $c_p^V(T)$, and $c_p^L(T)$ (evaluated at T_{tp}) that are listed in ref 38, since the values of these variables at the triple point are well-established. Thus, from the measured temperature gradients in the liquid and vapor phases (see Figure 3) the value of the local flux at the liquid−vapor interface may be calculated from eqs 14 and 15.

The values of the local flux obtained from the experiments performed with the PMMA funnel are listed in Table 1 where they are labeled ET1−ET3. The calculated mean-free-paths (MFP)[22] in the vapor phase during these experiments were 58, 50, and 39 μm, respectively. When the thermocouple was closest to the interface, the centerline of the thermocouple bead was within one MFP in each experiment. Thus, the molecules coming from the liquid phase would encounter the thermocouple, on average, at the same time as their first collision. The lowest liquid-phase temperature observed was 253.89 K when the vapor-phase pressure was 127 Pa.

4.1. Comparison with Previous Evaporation Experiments. The results reported from previous steady-state water evaporation experiments in which the interfacial temperature in the liquid and vapor phases were measured are listed in Tables 1–3.[18–21] These additional measurements were made under similar circumstances to the measurements described in the previous section, but the funnels used were either constructed of materials other than PMMA or had differently shaped mouth openings.

TABLE 2: Thermal Conditions in Liquid and Vapor Phases on the Funnel Centerline during Steady-State Evaporation[a]

experiment	vap phase pressure Pa	evap flux g/m^2 s	vap intf temp K	liq int temp K	intf radius R_1 mm	intf radius R_2 mm
EvC1	661.3	0.247	270.75	274.28	8.50	∞
EvC2	551.9	0.431	273.09	271.70	8.50	∞
EvC3	469.3	0.671	271.29	269.74	11.78	∞
EvC4	317.3	1.060	266.14	264.52	8.50	∞
EvC5	256.0	1.272	263.37	261.50	9.25	∞
EG1	596.0	0.2799	276.41	272.79	4.42	4.42
EG2	493.3	0.2544	273.81	270.19	4.39	4.39
EG3	426.6	0.3049	272.49	268.29	4.47	4.47
EG4	413.3	0.4166	272.09	267.89	4.27	4.27
EG5	310.6	0.3703	269.29	264.19	3.95	3.95
EG6	342.6	0.3480	270.39	265.39	4.31	4.31
EG7	333.3	0.3971	271.49	265.29	4.60	4.60
EG8	269.3	0.4081	268.49	262.39	4.36	4.36
EG9	277.3	0.4347	268.79	262.79	4.44	4.44
EG10	264.0	0.4097	268.19	262.09	4.15	4.15
EG11	269.3	0.4860	268.99	262.49	4.13	4.13
EG12	245.3	0.4166	267.09	261.19	4.12	4.12
EG13	233.3	0.4938	267.89	260.69	4.27	4.27
EG14	213.3	0.5086	266.89	259.59	4.17	4.17
EG15	194.7	0.5386	266.29	258.49	4.18	4.18

[a] Refs 18 and 21.

TABLE 3: Thermal Conditions in Liquid and Vapor Phases on the Funnel Centerline during Both Water Condensation (CP1−CP4) and Water Evaporation (EP1−EP4)[a]

experiment	vap phase pressure Pa	evap flux g/m^2 s	vap intf temp K	liq int temp K	intf radius R_1 mm	intf radius R_2 mm
CP1	3181	−0.266	299.2	298.8	7.119	7.119
CP2	2161	−0.130	292.7	292.4	4.545	4.545
CP3	1463	−0.118	286.2	285.8	6.690	6.690
CP4	959	−0.021	280.7	280.1	5.628	5.628
EP1	593	0.730	275.8	272.8	6.088	6.088
EP2	639	0.529	276.0	273.1	6.200	6.200
EP3	616	0.358	275.6	273.0	6.506	6.506
EP4	629	0.145	275.7	273.1	6.143	6.143

[a] Ref 19.

In the 19 experiments (EV1−EV19, Table 1) reported by Duan and Ward,[20] a stainless steel funnel of the same size and shape as the PMMA funnel was used. Otherwise, the two apparatuses were the same. The thermal conductivity of stainless steel is ∼79 times that of PMMA. The lowest liquid-phase temperature achieved with the stainless steel funnel experiments was 261.09 K; however, the water never froze in these experiments, even though the evaporation flux achieved with the stainless steel funnel was more than twice that achieved with the PMMA funnel. For the stainless steel funnel, the lowest pressure reached was limited by the vacuum system.

With the PMMA funnel, water could be held at 253.89 K and 127 Pa while it evaporated steadily. The lowest temperature reached was limited by ice nucleation. At 253.89 K and 127 Pa, the thermocouple mounted on a positioning micrometer could be dipped into the water and removed without initiating the formation of ice.

The five experiments labeled EvC1−EvC5 in Table 2 were reported in ref 21 and were performed with a stainless steel funnel, but rather than a circular mouth, the funnel mouth was a rectangular slot. As a result the liquid−vapor interface was cylindrically shaped. The curvature in the direction of the longitudinal cylinder axis vanished (infinite radius of curvature). The lowest liquid-phase temperature achieved in these experiments was 261.50 K at 256 Pa and is similar to that achieved when the liquid−vapor interface was spherical and maintained at the mouth of a stainless steel funnel 261.09 K, 259 Pa (Table 1, EV19). The evaporation fluxes at lowest temperatures were also similar: 1.272 and 1.205 g/m^2 s. However, when the liquid−vapor interface was cylindrical, the lowest temperature achieved was not limited by ice nucleation.

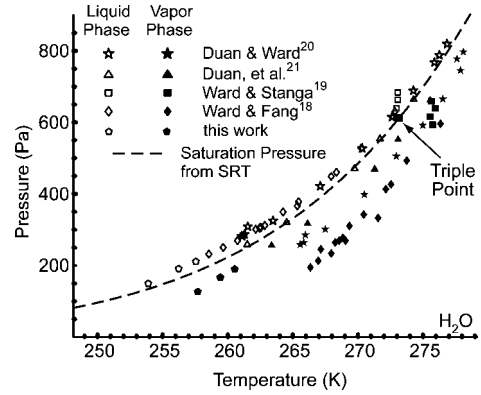

Figure 4. Nonequilibrium interfacial liquid and vapor temperatures and pressures for the evaporation experiments listed in Tables 1–3 are shown in this scatter plot. The dashed line is the saturation vapor pressure determined from measured nonequilibrium temperatures and pressures in the liquid and vapor phases using SRT, see eq 18.

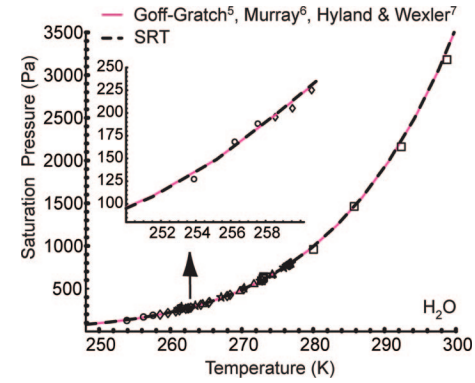

Figure 5. Calculated saturation vapor pressure from the measurements in Tables 1–3 and SRT.

The experiments labeled EG1−EG15 in Table 2 were performed using a borosilicate glass funnel with a circular mouth.[18] The thermal conductivity of glass is more than 6 times that of PMMA. Note that the lowest liquid-phase temperature observed was 258.49 K (EG15), and the corresponding evaporation flux was 0.5386 g/m^2 s. The lowest temperature observed during steady-state evaporation with a funnel of this material is less than that observed with the stainless steel funnels but greater than that observed with the PMMA funnel.

As the pressure in the vapor is raised, the evaporation flux can be reversed, producing condensation (negative value of j_{ev}). The results shown in Table 3 examined the conditions near the interface during both evaporation and condensation near the triple point.[19] The funnel used was constructed of PMMA and had a circular mouth opening of 7 mm diameter.

In each of the experiments listed in Tables 1–3, for both evaporation and condensation, the interfacial vapor temperature was greater than that of the liquid. The temperature discontinuity measured during evaporation experiment EG15 (Table 2) was the largest observed, 7.8 K. An interfacial temperature discontinuity is a feature of evaporation and condensation experiments with water.

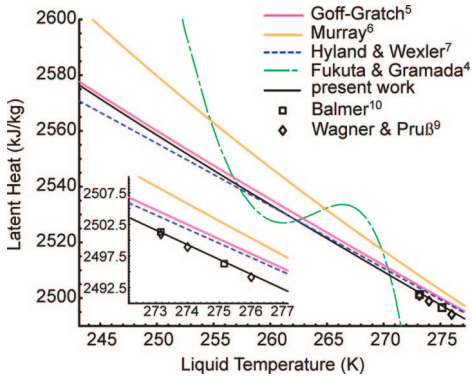

Figure 6. Comparison of the latent heat values calculated from the different analytical expressions for $P_s(T)$. The values obtained from the SRT expression, eq 10, are also shown. Note that there is no disagreement between the SRT calculations and the measurements.

4.2. Calculation of $P_s(T)$ from All of the Data. In Figure 4 a scatter plot is shown of the interfacial temperatures and pressures of the experiments listed in Tables 1–3. The open symbols indicate the conditions in the liquid phase and the filled ones, the conditions in the vapor. No information on the evaporation flux is shown in this figure; thus, there is no reason to expect this nonequilibrium data to indicate a correlation. For example, at one temperature several different pressures were observed. At each interfacial liquid temperature, the one property that these experiments should have in common is $P_s(T_I^L)$.

The data points shown in Figure 5 are values of $P_s(T_I^L)$ calculated from the measurements listed in Tables 1–3 using SRT (eqs 1, 10, 11, and 9) and the values of γ^{LV} and v_f given in refs 39 and 40, respectively:

$$\gamma^{LV} = 10^{-3}[75.47870 - 0.13848(T - 273.15) - 3.36392\times10^{-4}(T-273.15)^2 + 4.75362\times10^{-7}(T-273.15)^3 + 2.64479\times10^{-10}(T-273.15)^4] \quad (16)$$

$$v_f = 10^{-3}(334.601163 - 6.962367T + 6.067943\times10^{-2}T^2 - 2.825583\times10^{-4}T^3 + 7.411762\times10^{-7}T^4 - 1.038083\times10^{-9}T^5 + 6.0638484\times10^{-13}T^6) \quad (17)$$

Once the values of T_I^L, T_I^V, P_I^V, R_1, R_2, and j_{ev} for an experiment are inserted in the SRT equations, only $P_s(T_I^L)$ remains as an unknown, and its value may be determined from a numerical procedure. From these values of $P_s(T)$, an analytical expression for $P_s(T)$ may be determined:

$$P_s = 611.2\exp[1045.8511577 - 21394.6662629/T + 1.0969044T - 1.3003741\times10^{-3}T^2 + 7.7472984\times10^{-7}T^3 - 2.1649005\times10^{-12}T^4 - 211.3896559\ln(T)] \quad (18)$$

The calculated values of $P_s(T)$ obtained from eq 10 are shown in Figures 4 and 5 as the black dashed line.

The importance of including seven places after the decimal in the fitting relation obtained from SRT, eq 10, was assessed by calculating the average difference, $\overline{\delta P_s}$, in the values of $P_s(T)$ calculated from eq 18 and that determined from SRT using the experimental data listed in Tables 1–3. There are a total of 50 data points listed in these tables:

$$\overline{(\delta P_s)} = \frac{1}{50}\sum_{i=1}^{50}\left(\frac{\left|P_{si}^m - P_s(T_{Ii}^L)\right|}{P_s(T_{Ii}^L)}\right) \quad (19)$$

where P_{si}^m indicates the value determined from SRT at a particular T_{Ii}^L. The values of $(\overline{\delta P_s})$, obtained when different numbers of decimals were included in the coefficients of eq 18 are shown in Table 4. Note that when seven decimal places are included, the average error in the 50 data points is less than 1%. This does not suggest $P_s(T)$ is being determined to seven decimal places. As indicated in Tables 1–3, $P_s(T)$ is calculated to 0.1 Pa, but it is necessary to include seven decimal places in the constants of the fitting relation in order for it to have minimal disagreement with the values of $P_s(T)$ determined from SRT.

The data points in Figure 4 are those obtained from evaporation experiments listed in Tables 1–3 and SRT. Note that in each experiment the vapor was superheated and the liquid was supercooled. This result is consistent with assuming the vapor could be approximated as an ideal gas. The degree of superheating or supercooling is indicated by the distance of a data point from the $P_s(T)$ curve.

The data points in Figure 5 were obtained from both evaporation and condensation experiments. The solid red line was obtained from the expression for $P_s(T)$ proposed by Goff and Gratch,[5] by Murray,[6] and by Hyland and Wexler.[7] Note that on the scale of Figure 5 the difference between the predictions of $P_s(T)$ from the different analytical expressions is not visible, but as will be seen there are important differences in the slopes of these curves.

4.3. Calculation of the Latent Heat and the Constant Pressure Specific Heat. At all points on the $P_s(T)$ curve defined by eq 18, SRT requires eq 3 to be satisfied. If eq 3 is differentiated, the intensive entropies of the liquid and vapor phase at saturation are denoted s_f and s_g, and the corresponding specific volumes as v_f and v_g, one obtains the Gibbs−Duhem equation at the saturation condition:

$$-s_f\,dT + v_f\,dP_s = -s_g\,dT + v_g\,dP_s \quad (20)$$

After introducing the definition of the latent heat:

$$L_{lv}(T) \equiv T(s_g - s_f) \quad (21)$$

eq 20 may be written

$$L_{lv} = T(v_g - v_f)\frac{dP_s}{dT} \quad (22)$$

When eq 18 is used in eq 22, the latent heat may be calculated and is shown as the dark line in Figure 6. Also shown are the results obtained from expressions proposed for $P_s(T)$ by Goff and Gratch,[5,41] Murray,[6] Hyland and Wexler,[7] and Fukuta and Gramada.[4] Clearly the values obtained from SRT are in the best agreement with the data, but only the results obtained by Fukuta and Gramada can be said not to agree with the data of Wagner and Pruss[9] and Balmer.[10]

There is, unfortunately, limited data available for the latent heat, especially at lower temperatures, but as may seen in Figure 6 the different expressions for $P_s(T)$ predict different slopes for the latent heat. This allows further differentiation between the analytical expressions for $P_s(T)$, since the latent heat may also be written

$$L_{lv} = h_g - h_f \quad (23)$$

We neglect v_f compared to v_g, since the latter is 3 orders of magnitude larger than the former. The vapor phase has been approximated as an ideal gas; thus, the change in v_g with temperature is 7 orders of magnitude greater than that of v_f.

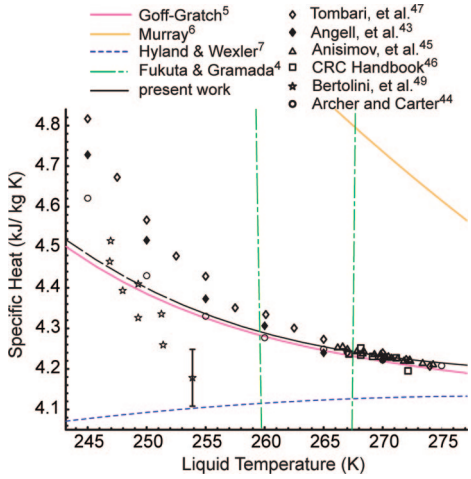

Figure 7. Comparison of the calculated values of the constant pressure specific heat of water, obtained from different analytical expressions for $P_s(T)$, with previous reported measurements.

TABLE 4: Validation of the Saturation Vapor Pressure Fitting Equation

no. of decimals	$\overline{\delta P_s}$ %
1	112.67
2	136.29
3	4.55
4	0.92
5	0.68
6	0.60
7	0.59

After combining eqs 21 and 22 and taking the partial differential with respect to T, one finds

$$c_p^{\mathrm{L}} = c_p^{\mathrm{V}} - \frac{\mathrm{d}}{\mathrm{d}T}\left(\frac{RT^2}{P_s}\frac{\mathrm{d}P_s}{\mathrm{d}T}\right) \quad (24)$$

The expression for $c_p^{\mathrm{V}}(T)$ has been previously established:[9,42]

$$c_p^{\mathrm{V}} = 10^{-3}(1875.811 - 3.465\times10^{-1}T - 5.919\times10^{-4}T^2 + 7.240\times10^{-6}T^3) \quad (25)$$

After eq 25 and an expression for $P_s(T)$ are substituted into eq 24, the indicated differential may be performed to obtain an expression for $c_p^{\mathrm{L}}(T)$ corresponding to each expression for $P_s(T)$. The results obtained from this procedure are shown in Figure 7.

5. Discussion

The value of the latent heat calculated from the expression for $P_s(T)$ proposed by Fukuta and Gramada[4] is clearly in disagreement with the data (see Figure 6), but the values of $L_{\mathrm{lv}}(T)$ calculated from the expressions proposed by Murray,[6] by Hyland and Wexler,[7] and by Goff and Gratch[5] differ from the measurements by less than 1%. The values obtained from the SRT expression are in complete agreement.

The measurements of $c_p^{\mathrm{L}}(T)$[43–47] are consistent only in the temperature range of 263 K $\leq T \leq$ 273 K, but in this temperature range, the values of c_p^{L} calculated from the proposed expressions for $P_s(T)$ by Fukuta and Gramada,[4] Hyland and Wexler,[7] and Murray[6] are not consistent with the data. By contrast, the calculations based on the Goff−Gratch equation[5] and those based on the expression for $P_s(T)$ obtained from SRT, eq 10, are not distinguishable from the data in this temperature range. This gives both of these expressions for $P_s(T)$ strong experimental support, at least for this range of temperatures.

Our measurements of $P_s(T)$ extend down to 253.9 K (see Table 1), and down to this temperature, there is no disagreement between the value of $c_p^{\mathrm{L}}(T)$ obtained from SRT and the measurements of Archer and Carter.[44] Also, the most recent measurements of $c_p^{\mathrm{L}}(T)$ reported by Angell et al.[43] (that were revised downward from their original report[48]) are not measurably different than the SRT values. Even the values reported by Tombari et al.,[47] in the temperature range of 253.9 K $\leq T \leq$ 273 K differ from the SRT values by less than 2%.

However, the disagreement comes when the SRT equation is used to calculate $c_p^{\mathrm{L}}(T)$ from 253.9 K down to 245 K. In this temperature range, the SRT calculations are shown as a dashed line in Figure 7. The data from four independent experimental investigations are not consistent. The data of Bertolini et al.[49] are a maximum of 4.3% below the SRT values and a maximum of 2% above. We note that Bertolini et al.[49] say that their data are in agreement with the measurements of Angell et al., but as indicated in Figure 7 their data actually fall well below the data that Angell et al. list as the "suggested" values for $c_p^{\mathrm{L}}(T)$. (The Bertolini data, shown in Figure 7, were taken from Figure 2 of ref 49.) The maximum deviation of the SRT value from the measurements of Archer and Carter[44] occurs at 245 K and is less than 3%.

In the temperature range of 253.9 down to 245 K, the values of $c_p^{\mathrm{L}}(T)$ reported by Angell et al. that were obtained with an emulsion technique[43] are greater than those calculated from the SRT equation. The accuracy of emulsion techniques has been discussed by Leyendekkers and Hunter,[50] and by Johari.[51] The former suggested the values of $c_p^{\mathrm{L}}(T)$ obtained by this technique are too large because of surface effects, and Johari also suggested the values may be too large, but because of "premelting". However, Johari was careful to point out an increase in $c_p^{\mathrm{L}}(T)$ with decreasing temperature is expected but is not expected to be as large as that indicated by the emulsion technique. His view seems to be consistent with the values of $c_p^{\mathrm{L}}(T)$ calculated from the SRT equation (see Figure 7). Also, the gentle increase in $c_p^{\mathrm{L}}(T)$ at lower temperatures does not support the proposal of a second critical point for water.[52]

Near 245 K, the largest values of $c_p^{\mathrm{L}}(T)$ are those reported by Tombari et al.,[47] but it is not clear how to interpret their results. Glass ampules were filled with samples of distilled water and cooled. Ten percent remained liquid down to 249 K, and $c_p^{\mathrm{L}}(T)$ was measured for two of these ampules. Clearly, the measurements are not typical of water. The authors suggested that it was the purity of these water samples that gave them this ability. However, there were no measurements indicating the purity, such as the resistivity or the surface tension. Also, since the water samples were each enclosed in a glass ampule, the transition to ice would have been impeded by a pressure rise.

Although the basis of the Goff−Gratch[5] expression for $P_s(T)$ is very different than the basis for the SRT expression, the two expressions are in surprisingly good agreement (see Figures 5–7). When either is used to predict $L_{\mathrm{lv}}(T)$ and $c_p^{\mathrm{L}}(T)$, the result cannot be said to be in disagreement with the measurements.

The temperature measurements listed in Table 1 were made with microthermocouples (bead diameter, ~45 μm). In the studies of refs 22 and 18 the temperature measurements, at positions where possible, were also made with a thermocouple that was approximately 3 times larger in diameter. No differences were found in the values obtained from the differently sized thermocouples. Thus, the temperature discontinuities measured at the interface during the phase-change processes

appear reliable. The strongest support for the validity of the temperature discontinuity measurements, to date, is the consistency of the SRT predictions of $L_{lv}(T)$ and $c_p^L(T)$ with independent measurements of these quantities.

The difference in the interfacial temperatures is one way to characterize the degree of disequilibrium between the liquid and the vapor phases during the evaporation process. If the system were in equilibrium T_I^L and T_I^V would have been the same, and if the slight curvature of the interface were neglected, the saturation vapor pressure would also have had the same value. With the use of eq 18, the difference in the saturation pressures $(P_s(T_I^V) - P_s(T_I^L))$ may be calculated. This measure of the degree of disequilibrium varied over a wide range in the experiments described in Tables 1–3. For example, in experiment CP2 (Table 2), the difference in the saturation pressures was 10 Pa, but in experiment EG15 (Table 2), the difference was 177 Pa. The SRT expressions for $L_{lv}(T)$ and $c_p^L(T)$ are in agreement with the measurements over the entire range of disequilibrium existing in these experiments, and there is no indication of it breaking down as the degree of disequilibrium is increased.

6. Summary and Conclusion

The saturation vapor pressure appears as a parameter in the SRT expression for the net evaporation flux. This allows $P_s(T)$ to be calculated over a range of temperatures below the triple point from measurements made at the water−vapor interface during either steady-state evaporation or condensation.

In the SRT approach, local equilibrium is assumed to exist at the interface in the liquid and in the vapor, but disequilibrium to exist between the phases. The transition probability concept is used to develop the expression for the net flux of molecules from the liquid to the vapor in terms of the instantaneous values of the independent intensive properties: μ_I^j/T_I^j and $1/T_I^j$ where j = L or V.[23] If the vapor is approximated as ideal and the liquid as essentially incompressible, statistical thermodynamics may be used to express these instantaneous properties in terms of the measureable interfacial temperatures and pressures. The expression for the net flux contains the saturation vapor pressure, $P_s(T_I^L)$, as a parameter, but importantly, it does not contain any other unknown parameters. All of the other parameters have been previously determined by others.

In the experiments considered, water either evaporated or condensed steadily while maintained at the mouth of a funnel constructed of different materials: borosilicate glass, stainless steel, or PMMA. All the temperature and pressure measurements were made on the centerline of a funnel. The flow fields in such funnels are assumed to be axisymmetric, so the centerline is a stagnation point for any surface tension-driven convection. This allows the evaporation flux on the centerline to be determined from an energy balance (see eq 14). Values of h_{fg}, c_p^L, and c_p^V, evaluated at the triple point where their values are well-established,[38] were used to determine the value of the net evaporation flux at this point. When this calculated value of the flux is equated to the SRT expression for the flux, the value of $P_s(T_I^L)$ may be determined, but since T_I^L was also measured, the value of the property P_s at 50 different temperatures was determined.

An analytical expression for $P_s(T)$ that accurately predicts the values determined experimentally is given in eq 18. A plot of $P_s(T)$ is shown in Figure 4 along with the data obtained from the evaporation experiments. Note that during the evaporation experiments the vapor was superheated and the liquid was supercooled. Since the vapor was subjected to a range of superheats, but the predictions obtained from SRT for L_{lv} and c_p^L are consistent with independent measurements of these properties (see Figures 6 and 7), this suggests that approximating the vapor as an ideal gas is reasonable.

In Figure 5, the $P_s(T)$ values obtained from eq 18 may be compared with the values obtained from both condensation and evaporation measurements. Also shown in this figure are the values obtained from other analytical expressions for $P_s(T)$. Although on the scale of this figure, the different analytical expressions for $P_s(T)$ appear very close, there are important differences in the predicted slope of $P_s(T)$. This difference becomes apparent when the expressions for $P_s(T)$ are used to predict L_{lv} and c_p^L. The predicted values of L_{lv} obtained from the different expressions for $P_s(T)$ are shown in Figure 6. Note that only the SRT expression for L_{lv} is in complete agreement with the available data.

The comparison of the SRT expression for c_p^L with the available data is more complex because the data are not consistent at lower temperatures, but down to temperatures of 265 K, the experimental data are consistent, and the SRT predictions are in complete agreement. The SRT predictions are not measurably different than the data presented by Archer and Carter[44] down to 250 K.

The most important assumption in the SRT approach is that the exchange rate between quantum states of different molecular configurations has the same value for all possible quantum states of an isolated system.[18] There are also other assumptions, such as the local equilibrium approximation in each phase at the interface, but all of these assumptions are examined to some degree by using the expression for $P_s(T)$ obtained from SRT to predict the values of L_{lv} and c_p^L that are measured independently.

The disequilbrium between the phases varied over a large range. The interfacial temperature discontinuity is one measure of the disequilibrium. This ranged from 7.8 in experiment EG15 to 0.3 in experiment CP2.

Acknowledgment. We wish to acknowledge the support of the Canadian Space Agency and the Natural Sciences and Engineering Research Council of Canada.

References and Notes

(1) Maron, S. H.; Lando, J. B. *Fundamentals of Physical Chemistry*; Macmillan, New York, 1974; p 630.
(2) Bottomley, G. A. *Aust. J. Chem.* **1978**, *31*, 1177–1180.
(3) Kraus, G. F.; Greer, S. C. *J. Phys. Chem.* **1984**, *88*, 4781–4785.
(4) Fukuta, N.; Gramada, C. M. *J. Atmos. Sci.* **2003**, *60*, 1871–1875.
(5) Goff, J. A.; Gratch, S. *Trans. Am. Soc. Heat. Vent. Eng.* **1946**, 95–122.
(6) Murray, F. W. *J. Appl. Meteorol.* **1967**, *6*, 203–204.
(7) Hyland, R. W.; Wexler, A. *ASHRAE Trans.* **1983**, *89*, 500–519.
(8) Murphy, D. M.; Koop, T. Q. *J. R. Meteorol. Soc.* **2005**, *131*, 1539–1565.
(9) Wagner, W.; Pruss, A. *J. Phys. Chem. Ref. Data* **2002**, *31*, 387–535.
(10) Balmer, R. T. In Thermodynamics; West Publishing Company: St. Paul, MN, 1990; p 775.
(11) Ward, C. A. *J. Chem. Phys.* **1983**, *79*, 5605–5615.
(12) Ward, C. A.; Findlay, R. D.; Rizk, M. *J. Chem. Phys.* **1982**, *76*, 5599–5605.
(13) Ward, C. A.; Rizk, M.; Tucker, A. S. *J. Chem. Phys.* **1982**, *76*, 5606–5614.
(14) Ward, C. A.; Tikuisis, P.; Tucker, A. S. *J. Colloid Interface Sci.* **1986**, *113*, 388–398.
(15) Tikuisis, P.; Ward, C. A. In *Transport Processes in Bubbles, Drops, and Particles*; Chhabra, R., DeKee, D. Eds.; Hemisphere Publishing Corp., New York, 1992; Chapter 5, pp 114−132.
(16) Elliott, J. A. W.; Ward, C. A. *J. Chem. Phys.* **1997**, *106*, 5667–5676.
(17) Ward, C. A.; Elliott, J. A. W. *Appl. Surf. Sci.* **2002**, *196*, 202–208.
(18) Ward, C. A.; Fang, G. *Phys. Rev. E* **1999**, *59*, 429–440.
(19) Ward, C. A.; Stanga, D. *Phys. Rev. E* **2001**, *64*, 051509.
(20) Duan, F.; Ward, C. A. *Phys. Rev. E* **2005**, *72*, 056302.

(21) Duan, F.; Badam, V. K.; Durst, F.; Ward, C. A. *Phys. Rev. E* **2005**, *72*, 056303.
(22) Fang, G.; Ward, C. A. *Phys. Rev. E* **1999**, *59*, 417–428.
(23) Ward, C. A. *J. Non-Equilib. Thermodyn.* **2002**, *27*, 289–303.
(24) Fang, G.; Ward, C. A. *Phys. Rev. E* **1999**, *59*, 441–453.
(25) McGaughey, A. J. H.; Ward, C. A. *J. Appl. Phys.* **2002**, *91*, 6406–6415.
(26) Dejmek, M.; Ward, C. A. *J. Chem. Phys.* **1998**, *108*, 8698–8704.
(27) Panczyk, T.; Rudzinski, W. *J. Phys. Chem. B* **2002**, *106*, 7846–7851.
(28) Torri, M.; Elliott, J. A. W. *J. Chem. Phys.* **1999**, *111*, 1686–1698.
(29) Rudzinski, W.; Plazinski, W. *J. Phys. Chem. B* **2006**, *110*, 16514–16525.
(30) Rudzinski, W.; Borowiecki, T.; Panczyk, T.; Dominko, A.; Gac, W. *Appl. Catal., A* **2002**, *224*, 299–310.
(31) Rudzinski, W.; Panczyk, T.; Plazinski, W. *J. Phys. Chem. B* **2005**, *109*, 21868–21878.
(32) Elliott, J. A. W.; Elmoazzen, H. Y.; McGann, L. E. *J. Chem. Phys.* **2000**, *113*, 6573–6578.
(33) Rudzinski, W.; Borowiecki, T.; Panczyk, T.; Dominko, A. *J. Phys. Chem. B* **2000**, *104*, 1984–1997.
(34) Ward, C. A.; Duan, F. *Phys. Rev. E* **2004**, *69*, 056308.
(35) Popov, S.; Melling, A.; Durst, F.; Ward, C. A. *Int. J. Heat Mass Transfer* **2005**, *48*, 2299–2309.
(36) Duan, F.; Ward, C. A. *Phys. Rev. E* **2005**, *72*, 056304.
(37) Herzberg, G. In *Molecular Spectra and Molecular Structure*; Van Nostrand: Princeton, NJ, 1964; Vol. 2, p 281.
(38) *Handbook of Chemistry and Physics*, 56th ed.; Weast, R. C. Ed.; Chemical Rubber Co.: Cleveland, OH, 1971; pp D180 , D122, D123.
(39) Feldkamp, K. *Chem.-Ing.-Tech.* **1969**, *41*, 1181–1183.
(40) Kell, G. S. *J. Chem. Eng. Data* **1967**, *12*, 66–69.
(41) Goff, J. A. *Trans. Am. Soc. Heat. Vent. Eng.* **1957**, 347–354.
(42) Liley, P. E. *Int. J. Mech. Eng. Educ.* **2005**, *33*, 45–50.
(43) Angell, C. A.; Oguni, M.; Sichina, W. J. *J. Phys. Chem.* **1982**, *86*, 998–1002.
(44) Archer, D. G.; Carter, R. W. *J. Phys. Chem. B* **2000**, *104*, 8563–8584.
(45) Anisimov, M. A.; Voronel', A. V.; Zaugol'nikova, N. S.; Ovodov, G. I. *JETP Lett.* **1972**, *15*, 317–319.
(46) *Handbook of Chemistry and Physics*, 56th ed.; Weast, R. C. Ed.; Chemical Rubber Co.: Cleveland, OH, 1971; p D159.
(47) Tombari, E.; Ferrari, C.; Salvetti, G. *Chem. Phys. Lett.* **1999**, *300*, 749–751.
(48) Angell, C. A.; Shuppert, J.; Tucker, J. C. *J. Phys. Chem.* **1973**, *77*, 3092–3099.
(49) Bertolini, D.; Cassettari, M.; Salvetti, G. *Chem. Phys. Lett.* **1985**, *119*, 553–555.
(50) Leyendekkers, J. V.; Hunter, R. J. *J. Chem. Phys.* **1985**, *82*, 1440–1446.
(51) Johari, G. P. *J. Chem. Phys.* **1997**, *107*, 10154–10165.
(52) Stanley, H. E.; Cruz, L.; Harrington, S. T.; Poole, P. H.; Sastry, S.; Sciortino, F.; Starr, F. W.; Zhang, R. *Physica A* **1997**, *236*, 19–37.

JP711768W